Microstructure Evolution During Al, Ti, and Mo Surface Deposition and Volume Diffusion in Ni-20Cr Wires and Woven Structures

CONG WANG and DAVID C. DUNAND

Ni-20 wt pct Cr wires, as individual wires or within 3D woven structures, are alloyed with Mo, Al, and Ti by gas-phase surface deposition and volume interdiffusion. Mo deposition creates Mo-rich coating and Kirkendall pores. Al + Ti co-deposition creates uniform triple-layered coating. The resulting homogenized and aged Ni-(17.4-19.6)Cr-(1.6-1.8)Al-(2.5-3.6)Ti-(1.5-4.5)Mo(wt pct) wires exhibit $\gamma + \gamma'$ superalloy microstructure. This demonstrates the feasibility of fabricating 3D woven Ni-base structures *via* gas-phase alloying and heat treatments, into multi-element superalloys with solid-state bonding at wire contacts.

DOI: 10.1007/s11661-015-2794-7
© The Minerals, Metals & Materials Society and ASM International 2015

I. INTRODUCTION

NOVEL architectured materials can be developed efficiently using topological optimization methods to predict ideal material architectures, and advanced 3D textile-based manufacturing, such as weaving and braiding, can fabricate large volumes of these periodic architectures, which may possess unusual combination of high permeability (thus heat transfer properties) and superior mechanical properties.[1–6] Successful fabrication of architecturally designed Ni-base superalloy woven structures is of particular interest to actively cooled structural materials operating in high-temperature, high-stress, oxidative, and corrosive environments, *e.g.*, shrouds, and load-bearing thermal management units including heat exchangers and heat pipes.[7–9]

The most direct route would be to braid and weave structures with wires made from the final, desired Ni-base superalloy. However, this approach is impractical as these alloys are not sufficiently ductile to be drawn into fine wires and/or to achieve the small bending radii needed for braiding. Thus, a novel four-step method is studied, where (i) ductile, commercial Ni or Ni-Cr wires are woven, taking advantage of their high ductility and low cost, (ii) they are then alloyed *via* surface deposition with further desirable elements, (iii) homogenized *via* annealing, and (iv) aged to create a desired microstructure. Often, steps (iii) and (iv) can be done in a single operation. Wire bonding is an optional step that can be carried out before, during, or after steps (ii to iii).[10,11]

Here, two methods are studied to alloy woven Ni-Cr structures into a superalloy composition. First, gas-phase deposition is used to add Al and Ti, which are the two main alloying elements necessary for the $\gamma + \gamma'$ superalloy microstructure. This process has already been demonstrated by chromization and aluminization of Ni-foams[12,13] and Ni or Ni-20Cr wires.[10,11,14–16] In a parallel trial, a refractory element, Mo, is also added by the same method to achieve superalloy compositions optimized for enhanced coarsening resistance, as recently demonstrated by us.[15,16]

We perform a systematic investigation to achieve the superalloy structure *via* sequential pack cementation of Mo, Al, and Ti on Ni-20Cr wires, either individually or as 3D woven structures. We show that samples in both cases develop significant amount of Kirkendall pores after Mo gas-phase deposition. By contrast, uniform triple-layered coatings are created after Al and Ti co-deposition without additional Kirkendall porosity. Upon homogenization and aging, the layered coatings dissolve and diffuse into the wire until full homogenization is reached, and the desired $\gamma + \gamma'$ microstructure is created. The successful implementation of the in situ alloying technique paves the way for creating architecturally designed woven or braided superalloy structures combining unusual pairs of properties, such as high permeability and high-specific stiffness or strength.

II. EXPERIMENTAL PROCEDURES

A. *Pack Cementation*

Raw materials employed in this study were procured from Alfa Aesar and include: Ni-Cr individual wires (Ni-20Cr-1Si-0.5Fe, wt pct, $d = 143$ μm) as substrate; Al_2O_3 powder (20 to 50 μm particle size) as inert filler; NH_4Cl powder (100 μm particle size) as halide source; and metal sources, *i.e.*, Mo powder (2 to 7 μm particle size), Ni-50 wt pct Al powders (150 μm particle size) and pure Ti powders (44 μm particle size).

CONG WANG, Professor, formerly with the Department of Materials Science and Engineering, Northwestern University, Evanston, IL, 60208, is now with the College of Materials and Metallurgy, Northeastern University, Shenyang 110819, P.R. China. Contact e-mail: wangc@smm.neu.edu.cn DAVID C. DUNAND, Professor, is with the Department of Materials Science and Engineering, Northwestern University.

Manuscript submitted August 20, 2014.
Article published online February 18, 2015

The non-crimp 3D orthogonal woven structure was made by Saertex (Huntersville, NC) from soft-annealed Chromel A wires (Ni-20Cr-1Si-0.5Fe, wt pct, d = 202 μm) and had an average 3.2-mm thickness and a fill insertion spacing of 0.7 ± 0.02 mm. The metal volume fraction was 11.6 pct in the warp, 12.0 pct in the fill, and 9.1 pct in the Z directions for a total metal volume fraction of 32.7 pct. Detailed weaving fabrication specifications and procedures are presented in (References 6 through 11) Specimens were cut into 10 × 10-mm coupons with a diamond saw.

Pack cementation experiments were conducted in a tube furnace under argon flow at 1273 K (1000 °C). Detailed procedures can be found elsewhere.[11,15] For both the individual wire and woven structure experiments, Mo pack cementation took place first, with replenished feedstock (3 wt pct NH_4Cl, 40 wt pct Mo and 57 wt pct Al_2O_3) at 1-hour interval, for eight cycles. Subsequently, the Mo-alloyed wires were homogenized at 1373 K (1100 °C) for 48 hours in a high-vacuum furnace terminated by furnace fast cooling (50 °C/minutes). Following this step, alumo-titanization was performed for 10 minutes. For both cases, after Al and Ti co-deposition, samples were homogenized at 1373 K (1100 °C) for 24 hours and subsequently at 1473 K (1200 °C) for 1 hour, in a high-vacuum furnace, after which the samples were cooled down at 50 °C/minutes. Homogenization was followed by an aging treatment at 1273 K (1000 °C) for 12 hours to induce the $\gamma + \gamma'$ superalloy structure. This final step was also terminated by fast furnace cooling (50 °C/minutes) to room temperature.

B. *Characterization*

Specimens were mounted in epoxy, and then ground and polished down to 0.05 μm colloidal alumina by standard procedures. Selected polished cross sections were etched by a solution composed of 33 vol pct D.I. water, 33 vol pct nitric acid, 33 vol pct acetic acid, and 1 vol pct hydrofluoric acid. The microstructure was investigated by a Hitachi SU8030 scanning electron microscope (SEM) at an acceleration voltage of 15 kV. Compositional analysis was completed with an energy-dispersive X-ray spectrometer (EDS), which was calibrated by standard samples of Ni with accuracy of ±1 pct.

Micro-Vickers hardness tests were performed on polished cross sections of both wire and woven samples using a Struers Duramin5 tester by applying a 136 deg pyramidal diamond indenter under a load of 50 g for 5 seconds. At least six measurements were obtained for each sample and the average value and error range are reported.

III. RESULTS AND DISCUSSION

A. *Ni-Cr Wires*

Figures 1(a) through (h) show the microstructural development of individual Ni-Cr wires after pack cementation, homogenization, and aging. Figure 1(a), a cross-sectional view of the Ni-Cr wire after 8-hours Mo deposition, shows that a ~20-μm thick Mo-rich coating has formed, containing up to 9.3 wt pct Mo. In addition, significant amount of pores have been created as a result of the Kirkendall effect due to Mo/Ni/Cr interdiffusion. Indeed, interdiffusion coefficients[17,18] show that Ni and Cr diffuse in nickel more rapidly than Mo, creating an outward net radial flux of Ni and Cr atoms, leaving vacancies in the Ni-Cr matrix which coalesce into pores. The Kirkendall effect has also been reported for pure Ni wires into which Mo was deposited by pack cementation[16]

In Figure 1(b), where the Mo-deposited Ni-Cr wire has been fully homogenized at 1373 K (1100 °C) for 48 hours, it is apparent that the Kirkendall pores have sintered and coalesced to form fewer, larger cavities. Ni, Cr, and Mo are uniformly distributed across the wire, as demonstrated by the EDS line scan, indicating full homogenization. The average Mo content is 4.5 ± 0.7 wt pct. Co-depositing Al + Ti onto the homogenized Ni-Cr-Mo alloy at 1273 K (1000 °C) for 10 minutes results in the formation of the Al- and Ti-rich coatings, as demonstrated in Figure 1(c). A higher magnification view of the coating in Figure 1(d) reveals that it is composed of three distinctive layers, *i.e.*, an outer Ni_2AlTi shell, an intermediate Ni_3AlTi shell, and an inner Cr rejection layer within the Ni-Cr matrix.

Figure 1(e) shows that the triple-layered coating disappears, after further homogenization at 1373 K (1100 °C) for 24 hours. EDS measurements show that the Al and Ti contents are 1.8 ± 0.4 and 2.5 ± 0.6 wt pct, respectively, and are uniform across the cross section. Mo content remains constant at ~ 4.5 wt pct, as expected from the low vapor pressure of Mo. It is also apparent that the Kirkendall pores have not sintered appreciably after this heat treatment. Comparison with previous states is made difficult, as it is possible that the Kirkendall pores are distributed unevenly along the wire length. Thus, the unexpected result that the cross section presented Figure 1(c), which is before homogenization, shows a reduced porosity as compared to Figure 1(e), may disappear if porosity was measured over large volumes, *e.g.*, by tomography, rather than on individual cross sections.

Further etching of the homogenized Ni-Cr-Mo-Al-Ti wire (Figure 1(f)) reveals that it consists of an outer shell of coarse γ' grains, and a core region (Figure 1(g)), where γ' submicron precipitates are distributed in the γ matrix. This indicates that the homogenization temperature of 1373 K (1100 °C) is too low to fully solutionize the alloy and that γ' precipitation occurred at the later stage of the 1373 K (1100 °C) heat treatment, once the interdiffusion had erased concentration gradients in the wire. From image analysis, γ' precipitates have a volume fraction ~17 pct with sizes ranging from 20 to 150 nm. According to the systematical studies by Loomis *et al.*[19] and Maniar *et al.*[20] of compositionally similar alloys, our homogenization temperature is close to the solvus temperature range, so that extended annealing can promote the formation of γ'.

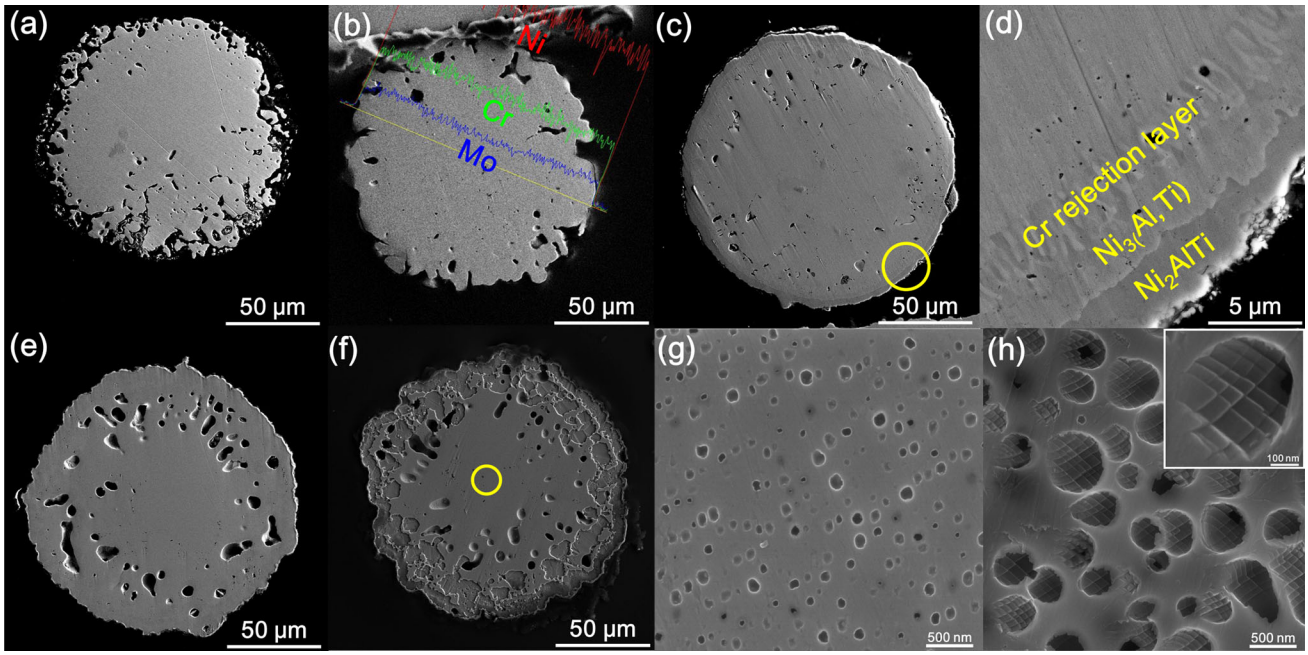

Fig. 1—Series of SEM micrographs showing the microstructure development in cross sections of Ni-Cr individual wires. (*a*) Ni-Cr wire after 8-h Mo deposition showing extensive Kirkendall porosity, (*b*) Ni-Cr-Mo wire after homogenization, with coarsened pores; EDS line scan over the wire diameter shows uniform distributions of Ni, Cr, and Mo, (*c*) Ni-Cr-Mo wire after Al + Ti co-deposition, (*d*) enlarged illustration of coated area circled in (c) with three distinctive layers present on the Ni-Cr wire, consisting of an outer shell of Ni_2AlTi, a middle shell of $Ni_3(Al,Ti)$, and an inner Cr rejection layer, (*e*) Ni-Cr-Mo-Al-Ti wire after homogenization at 1373 K (1100°C) for 24 h, (*f*) homogenized Ni-Cr-Mo-Al-Ti wire [same as in (e)] after etching showing serrated boundary between the γ' outer shell and $\gamma + \gamma'$ core, (*g*) $\gamma + \gamma'$ superalloy structure from the core region inset circled in (f), and (*h*) $\gamma + \gamma'$ structure after homogenization at 1473 K (1200 °C) for 1 h followed by aging at 1273 K (1000 °C) for 12 h. Inset shows an enlarged image of a coarsened γ' precipitate demonstrating layered and striated features.

To induce a larger fraction of γ' precipitates which is desirable for creep resistance,[21] an aging treatment at 1273 K (1000 °C) was added for 12 hours, after increasing the homogenization temperature to 1473 K (1200 °C) for 1 hour to fully solutionize the alloy. The final representative microstructure, shown in Figure 1(h), illustrates that γ' precipitates are present with a higher volume fraction (52 pct) and larger size (50 to 720 nm) than when precipitation occurs in the later stage of the 1373 K (1100 °C) annealing (Figure 1(g)). The apparent contradiction of coarser precipitates at lower temperature [1273 K (1000 °C) *vs* 1373 K (1100 °C)] and shorter times (12 *vs* 24 hours) can be explained by the fact that a large fraction of the 24 hours was not available for precipitation and coarsening of the γ' precipitates, as the Al and Ti gradients were still being equilibrated during the interdiffusion. The precipitates in Figure 1(h) show spheroidal shape, and in some cases are split into layered and striated structures (see insert in Figure 1(h)), which might be due to morphological instability from lattice misfit during coarsening.[22–25]

B. *Ni-Cr Woven Structure*

The non-crimp 3D Ni-Cr woven structures were treated in the same sequence as for the individual wires. The sequential development of the microstructures is shown in Figure 2. It is noted that since the woven structure contains five layers in warp (length) and six layers in fill (width), a significant amount of wires, both near the core and near the surface of the structure, are characterized and representative microstructures are presented.

Figure 2(a) demonstrates the effect of Mo vapor phase deposition on the Ni-Cr woven structure. Kirkendall pores have been created on both sides of the wire, and to depths of ~45 μm, as compared to ~50 μm for individual wires. Since the weave wire diameter is nearly twice that of the individual Ni-Cr wires, the majority of the wire inner volume remains free of pores. As shown in Figure 2(b), the subsequent homogenization step at 1373 K (1100 °C) for 48 hours drives the pore to sinter and coalesce, and, most importantly, makes the distribution of Mo and Cr uniform along the wire diameter, as shown by the EDS line scan. However, the Mo content is 1.5 ± 0.3 wt pct, significantly less than that of counterpart from the individual Ni-Cr wire (4.5 ± 0.7 wt pct). Two likely reasons are that (i) there is more total wire mass in the woven structures for the same amount of pack, and (ii) the gaseous Mo halide does not penetrate fully into the woven structure, which is not as exposed as bare individual Ni-Cr wires. In small regions in the center of the woven structure, Mo content in the wires is near zero due to this shielding effect. Cementation under pressurized conditions[11] may help alleviate this issue.

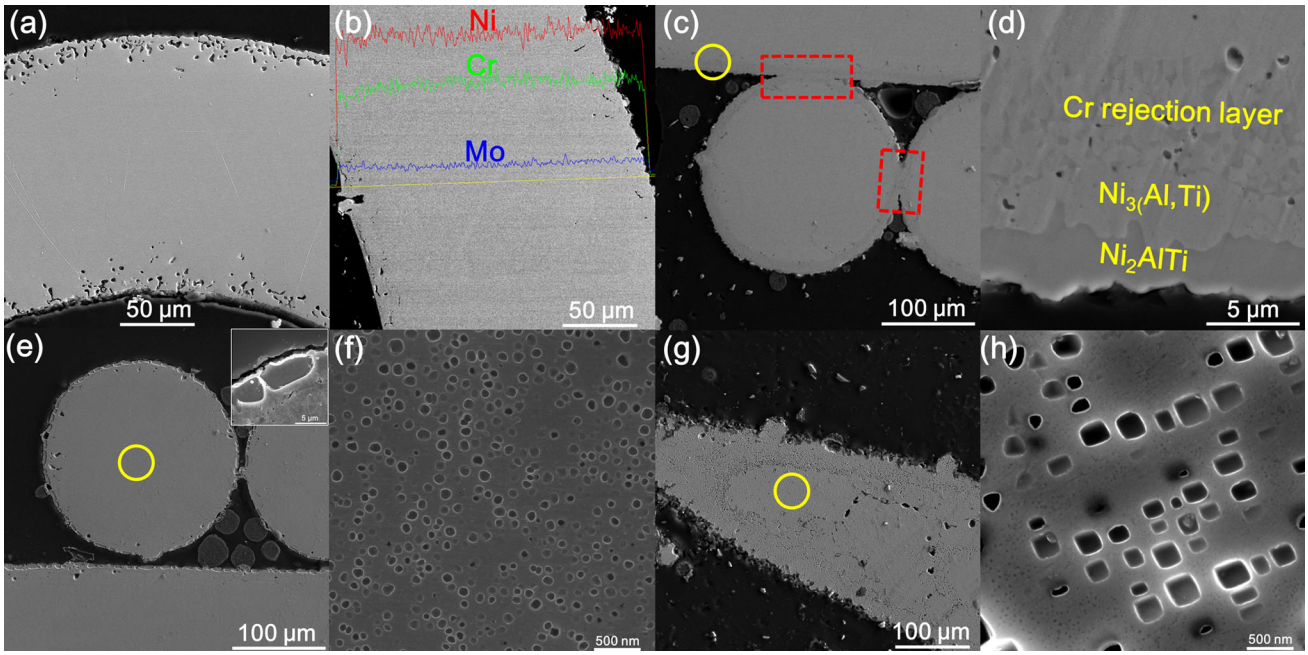

Fig. 2—Series of SEM micrographs showing the microstructure development in cross sections of Ni-Cr woven structures. (*a*) Ni-Cr wire after 8-h Mo deposition with Kirkendall pores near wire surface, (*b*) Ni-Cr-Mo alloy after homogenization; EDS line scans show uniform distributions of Ni, Cr, and Mo, (*c*) Ni-Cr-Mo after Al + Ti co-deposition; red boxes show where the coating layers impinge on each other, forming a metallurgical bond between adjacent wires, (*d*) higher magnification view of the coated area circled in (c) with three distinctive layers consisting of an outer shell of Ni_2AlTi, a middle shell of $Ni_3(Al,Ti)$, and an inner Cr rejection layer, (*e*) Ni-Cr-Mo-Al-Ti wire after homogenization at 1373 K (1100 °C) for 24 h; inset figure shows the γ' outer shell, (*f*) $\gamma + \gamma'$ superalloy structure obtained from the etched Ni-Cr-Mo-Al-Ti wire core region inset circled in (e), (*g*) Ni-Cr wire after homogenization at 1473 K (1200 °C) for 1 h followed by aging at 1373 K (1000 °C) for 12 h, and (*h*) $\gamma + \gamma'$ structure from circled region in (g) with γ' precipitates showing ordering features.

Similarly, after Al + Ti co-deposition, wires from the woven structure are coated with triple-layered coatings (Figures 2(c) through (d)). Thicknesses of respective coatings are uniform throughout the woven sample and comparable with those obtained from the Ni-Cr individual wires. In some regions, the coatings are found to be connected to each other (denoted by dashed red boxes), indicating the formation of metallurgical bonding between the wires. Such bonds are desirable as they enhance the strength and stiffness of the weave while reducing only marginally its permeability. They have been previously reported in 3D Ni-Cr woven structures aluminized under pack cementation.[11]

Homogenization of the Al + Ti-co-deposited woven structure at 1373 K (1100 °C) for 24 hours leads, as for the Ni-Cr individual wires, to the formation of an outer shell composed of γ' grains (Figure 2(e)), and, in the inner core of the wire, γ' precipitates in a γ matrix (Figure 2(f)). The γ' precipitates take up a volume fraction of 31 pct, which is higher than the value of ~17 pct for the individual wires after this stage. This increase in γ' volume fraction is consistent with the higher Al + Ti content, which is 5.2 wt pct for the woven structures and 4.3 wt pct for the individual wires. Additionally, the different Mo content (1.5 *vs* 4.5 wt pct) affects the γ' solvus temperature[19] and thus both thermodynamics and kinetics of γ' precipitation. The γ' precipitates exhibit spherical morphology and their sizes vary from 40 to 120 nm, similar to those of γ' precipitates in individual wires.

Figures 2(g) and (h) show that the Ni-Cr-Mo-Al-Ti woven structure was further homogenized at 1473 K (1200 °C) for 1 hour and aged at 1273 K (1000 °C) for 12 hours. Two changes occur as compared to the 1373 K (1100 °C) treatment: (i) the morphology of γ' precipitates is cuboidal rather than spheroidal, and (ii) the γ' precipitates are larger, with a majority >200 nm. However, there is no appreciable volume fraction change. Final Al and Ti contents of the woven structure are 1.6 ± 0.4 and 3.6 ± 0.5 wt pct, respectively, which are close to those determined from the individual wire. The Mo content is 1.5 ± 0.3 wt pct Mo, as compared to 4.5 ± 0.7 wt pct for the individual wires. Mo difference may explain the different shape: in a similar alloy containing 1.0 wt pct Al and 3.5 wt pct Ti, it was reported that reduced Mo content from 8 to 2 wt pct[26] will change the morphology of γ' precipitates from spheroidal to cuboidal as lattice-parameter mismatch increases in magnitude and as the cuboidal shape lowers the strain energy for coherent precipitates.[19]

C. *Hardness Evolution*

Figure 3 presents hardness values after each major processing stage, which is marked by respective alloying status, to explore the effects of Mo addition, Al + Ti deposition, and γ' precipitation.

For both cases, the as-received Ni-Cr alloy shows hardness value of ~170 HV (167 ± 3 HV, wire; 171 ± 3 HV, woven structure), which is consistent with

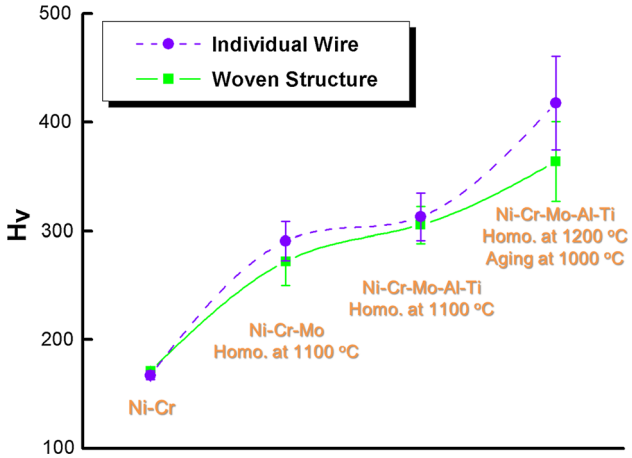

Fig. 3—Hardness evolution of Ni-Cr individual wires and woven structures after each processing step.

values from literature.[10] After Mo pack cementation and 48-hour homogenization, Mo diffuses into the wire and woven structure, and significantly enhances their hardness. For the individual Ni-Cr wire, the hardness value reaches 291 ± 18 HV, while that of woven structure is 272 ± 22 HV. These values are almost twice that of the as-received Ni-Cr alloy, reflecting the solid-solution strengthening effect of Mo in the Ni-Cr matrix.[19] The hardness value of the individual wire is slightly higher than that of the woven structure, which is likely due to the Mo content difference (4.5 *vs* 1.5 wt pct). The relatively large error ranges for both cases may be ascribed to Kirkendall pores, which, although coalesced after homogenization, may still present under the cross section and may affect indentation readings.

After Al + Ti co-deposition and homogenization/aging at 1373 K (1100 °C) for 24 hours, hardness values for Ni-Cr individual wires and woven structures increase to 313 ± 22 and 306 ± 17 HV, respectively. The γ' precipitates formed in the γ matrix (Figures 1(g), 2(f)) are responsible for this additional strengthening. Upon the alternate aging at 1273 K (1000 °C) for 12 hours, the hardness value for the Ni-Cr individual wire jumps to 418 ± 43 HV and that of woven structure to 364 ± 37 HV. These increases, as compared to the 1373 K (1100 °C) aging, reflect the higher volume fractions of coarser γ' precipitates, as shown in Figures 1(h) and 2(h), respectively. Hardness difference between individual and woven wires is likely due to the Mo content difference (4.5 *vs* 1.5 wt pct, respectively), as higher Mo content leads to increased volume fraction of γ' precipitates[20] and higher solid-solution strengthening of γ where the Mo tends to segregate.[27] Mo is also expected to decrease the coarsening of γ' precipitates, which is desirable for long exposure times at elevated temperature.[20]

IV. CONCLUSIONS

Vapor phase deposition of Mo, Al, and Ti has been applied on Ni-20Cr wires, both individually and woven into non-crimp orthogonal 3D structures. Mo induces Kirkendall pores and a Mo-rich coating, while Al + Ti co-deposition results in triple-layered coatings without Kirkendall pores. Upon subsequent Mo and Al + Ti homogenization, a gradient-free Ni-(17.4-19.6)Cr-(1.6-1.8)Al-(2.5-3.6)Ti-(1.5-4.5)Mo (wt pct) is created, in which γ' precipitates are formed upon aging. Mo affects the alloy both by solid-solution strengthening and by modifying the γ' particle shape and volume fraction.

We have demonstrated here that fabrication of 3D-woven, nickel-base superalloy structures is possible *via* gas-phase alloying and heat treatments for multi-element compositions typical of modern superalloy compositions. These architecturally designed woven superalloy structures can be topologically optimized for a combination of high permeability and strength/stiffness, while exhibiting the benefits of superalloys (*e.g.*, resistance to high temperature, creep deformation, corrosion, and oxidation).

ACKNOWLEDGMENTS

Financial support from the Defense Advanced Research Projects Agency (DARPA) under award number W91CRB1010004 monitored by Dr. Judah Goldwasser is acknowledged. The authors also thank Dr. Dinc Erdeniz and Ms. Ashley Paz y Puente (both of Northwestern University) for useful discussions.

REFERENCES

1. T.A. Schaedler, A.J. Jacobsen, A. Torrents, A.E. Sorensen, J. Lian, J.R. Greer, L. Valdevit, and W.B. Carter: *Science*, 2011, vol. 334, pp. 962–65.
2. J.K. Guest and J.H. Prevost: *Int. J. Solids Struct.*, 2006, vol. 43, pp. 7028–47.
3. H.N.G. Wadley, N.A. Fleck, and A.G. Evans: *Compos. Sci. Technol.*, 2003, vol. 63, pp. 2331–43.
4. D.J. Sypeck and H.N.G. Wadley: *J. Mater. Res.*, 2001, vol. 16, pp. 890–97.
5. Y.-H. Lee, B.-K. Lee, I. Jeon, and K.-J. Kang: *Acta Mater.*, 2007, vol. 55, pp. 6084–94.
6. K. Sharp, D. Mungalov, and J. Brown: *Proc. Mater. Sci.*, 2014, vol. 4, pp. 19–24.
7. S.J. Johnson, B. Tryon, and T.M. Pollock: *Acta Mater.*, 2008, vol. 56, pp. 4577–84.
8. Q.M. Zhang and X.D. He: *Mater. Charact.*, 2009, vol. 60, pp. 178–82.
9. D.E. Burns, Y. Zhang, M. Teutsch, K. Bade, J. Aktaa, and K.J. Hemker: *Scripta Mater.*, 2012, vol. 67, pp. 459–62.
10. D. Erdeniz and D.C. Dunand: *Intermetallics*, 2014, vol. 50, pp. 43–53.
11. D. Erdeniz, A.J. Levinson, K.W. Sharp, D.J. Rowenhorst, R.W. Fonda, and D.C. Dunand: *Metall. Mater. Trans. A*, DOI: 10.1007/s11661-014-2602-9.
12. A.M. Hodge and D.C. Dunand: *Intermetallics*, 2001, vol. 9, pp. 581–89.
13. H. Choe and D.C. Dunand: *Acta Mater.*, 2004, vol. 52, pp. 1283–95.
14. D.C. Dunand, A.M. Hodge, and C. Schuh: *Mater. Sci. Technol.*, 2002, vol. 18, pp. 326–32.
15. C. Wang and D.C. Dunand: Unpublished research.
16. C. Wang and D.C. Dunand: *Metall. Mater. Trans. A*, 2014, vol. 45A, pp. 6252–59.
17. C.E. Campbell, W.J. Boettinger, and U.R. Kattner: *Acta Mater.*, 2002, vol. 50 (4), pp. 775–92.
18. V.D. Divya, U. Ramamurty, and A. Paul: *Metall. Mater. Trans. A*, 2012, vol. 43A, pp. 1564–77.

19. W.T. Loomis, J.W. Freeman, and D.L. Sponseller: *Metall. Trans.*, 1972, vol. 3, pp. 989–1000.
20. G.N. Maniar, J.E. Bridge, Jr, and H.M. James: *Metall. Trans.*, 1971, vol. 2, pp. 1484–87.
21. G.N. Maniar and J.E. Bridge, Jr: *Metall. Trans.*, 1971, vol. 2, pp. 95–102.
22. A.G. Khachaturyan, S.V. Semenovskaya, and J.W. Morris, Jr: *Acta Metall.*, 1988, vol. 36, pp. 1563–72.
23. M.J. Kaufman, P.W. Voorheres, W.C. Johnson, and F.S. Biancaniello: *Metall. Trans. A*, 1989, vol. 20A, pp. 2171–75.
24. Y.S. Yoo: *Scripta Mater.*, 2005, vol. 53, pp. 81–85.
25. N. Ratel, G. Bruno, and B. Deme: *J. Phys.*, 2005, vol. 17, pp. 7061–75.
26. V. Biss and D.L. Sponseller: *Metall. Trans.*, 1973, vol. 4, pp. 1953–59.
27. Y. Tu, Z. Mao, and D.N. Seidman: *Appl. Phys. Lett.*, 2012, vol. 101, p. 121910.